SSC-132

THE FEASIBILITY OF X-RAY INSPECTION OF WELDS USING BACK SCATTERED RADIATION

by

E. L. Criscuolo

C. H. Dyer

and

D. P. Case

SHIP STRUCTURE COMMITTEE
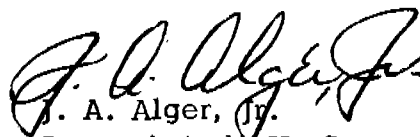
SHIP STRUCTURE COMMITTEE

July 28, 1961

Dear Sir:

As part of its research program related to the fabrication of hull structures of ships, the Ship Structure Committee sponsored a study at the U. S. Naval Ordnance Laboratory to try to develop a radiographic flaw detection technique using source and film located on the same side of the plate. Herewith is a copy of the final report, SSC-132, The Feasibility of X-Ray Inspection of Welds Using Back Scattered Radiation by E. L. Criscuolo, C. H. Dyer, and D. P. Case.

This project was conducted under the advisory guidance of the Ship Structure Subcommittee.

Distribution of this report is being made to those individuals and agencies associated with and interested in the work of the Ship Structure Committee. Questions or comments pertaining to the report should be addressed to the Secretary, Ship Structure Committee.

Sincerely yours,

J. A. Alger, Jr.
Rear Admiral, U. S. Coast Guard
Chairman, Ship Structure Committee

Serial No. SSC-132

Final Report
of
Project SR-159

to the

SHIP STRUCTURE COMMITTEE

on

THE FEASIBILITY OF X-RAY INSPECTION OF WELDS
USING BACK SCATTERED RADIATION

by

E   L. Criscuolo, C. H   Dyer, and D   P. Case

U. S. Naval Ordnance Laboratory
White Oak, Silver Spring, Maryland

ABSTRACT

Theoretical and experimental work was conducted to develop a radiographic flaw detection technique using source and film located on the same side of the plate.

In view of a serious limitation on the depth at which discontinuities in steel can be detected (0.20 in.) and long exposure time (20 min. at 250 kv), the method is considered to be unsatisfactory as a critical inspection tool.

CONTENTS

SR-159 PROJECT ADVISORY COMMITTEE

"Radiographic Techniques"

for the

SHIP STRUCTURE SUBCOMMITTEE

Chairman:

D. T. O'Connor
Machlett Laboratories, Inc.

Members:

Samuel Baum
Ship Welding Engineer
Philadelphia Naval Shipyard

C. H. Hastings
AVCO Corp.
Research & Advanced Development Division

R. D. Karl, Cdr., USN
Director of the Engineering Division
Maintenance and Repair, M.S.T.S.

INTRODUCTION

General

The applicability of radiography for the inspection of welds has been well established. This method, utilizing isotopes or portable X-ray equipment is suitable for field inspection where both sides of a weld are accessible. It would be desirable to have a radiographic inspection method requiring access to only one side of a weld, since in many cases during field inspection one side of a weld is inaccessible. A previous study by Bujes[1] indicated that scattered radiation could be utilized for this purpose. This proposed method makes use of an isotope and a scintillation detector. The weld is irradiated with the isotope and the detector is collimated so that the back scatter from each point of the weld can be detected. The intensity of the scattered radiation must then be analyzed to find the defects. Although less sensitive, a pictorial method[2] of presentation might give more over-all information. By substituting a pinhole camera for the scintillation detector, the scattered radiation generated from the weld area can be imaged on film.

Purpose of Investigation

In view of the success achieved by Dr. Bujes with his preliminary experiments on scattered radiation, it seemed desirable to investigate application of this method with a pinhole camera to record the image. This investigation, under the sponsorship of the Ship Structure Committee, was aimed at gathering sufficient information to evaluate the method as a possible inspection technique for welds in steel.

THEORETICAL CONSIDERATIONS OF IMAGING BY SCATTERED RADIATION

General

An object irradiated by an X-ray beam produces various intensities of radiation in all directions. The back scatter radiation, which has a longer wave length than the primary beam, is partially absorbed by the object; therefore, a measurement of the attenuation of this scatter by a scintillation counter, ion

chamber, or film permits the detection of a void within the object.

By collimation the detector receives radiation from a small surface area of the object. A void below the surface allows more of the scatter radiation originating at a greater depth to reach the surface; therefore, by scanning the surface of the object under inspection, information is obtained on the location of the voids. A sketch of such an inspection arrangement is shown in Fig. 1(a). If a pinhole camera is substituted for the detector, as shown in Fig. 1(b), an image of the object will be produced. Although the pinhole camera requires long exposure times, it covers a large area at a single exposure.

Intensity from a Flat Plate

Figure 2(a) illustrates a situation for scattered radiation generated from a plate. The intensity from the irradiating source is shown as I_p and scatter from the plate as I_s. In practice, I_p and I_s are at an angle with respect to the plate. For simplification, I_p and I_s are shown at right angles to the surface of the plate; therefore, in the development of the equations, no consideration will be given to the angles.

The primary beam penetrating the plate is attenuated according to the classical absorption law:

$$I = I_o e^{-\mu x}$$

where

I_o = primary intensity

μ = linear absorption coefficient

x = thickness of absorber

The back scatter is also attenuated in the same manner. The scatter radiation arises from each elemental unit Δx in the absorber. The following relation can be deduced from Fig. 2(a).

$$\Delta I_s = I_p \text{ (absorption of primary beam)(generation of scatter)} \text{ (absorption of scatter)}$$

$$\Delta I_s = I_p (e^{-\mu_p x})(\mu_c \Delta x)(e^{-\mu_s x})$$
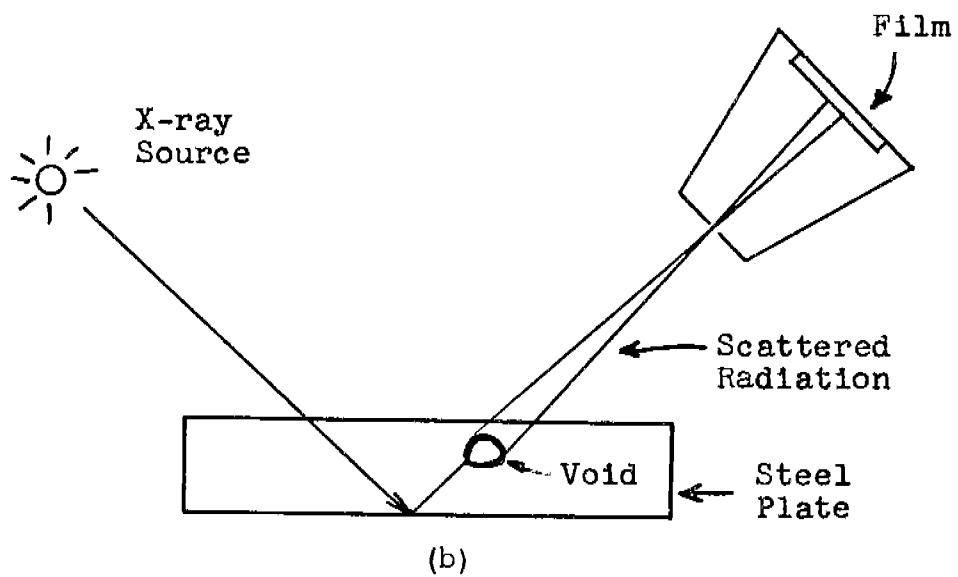
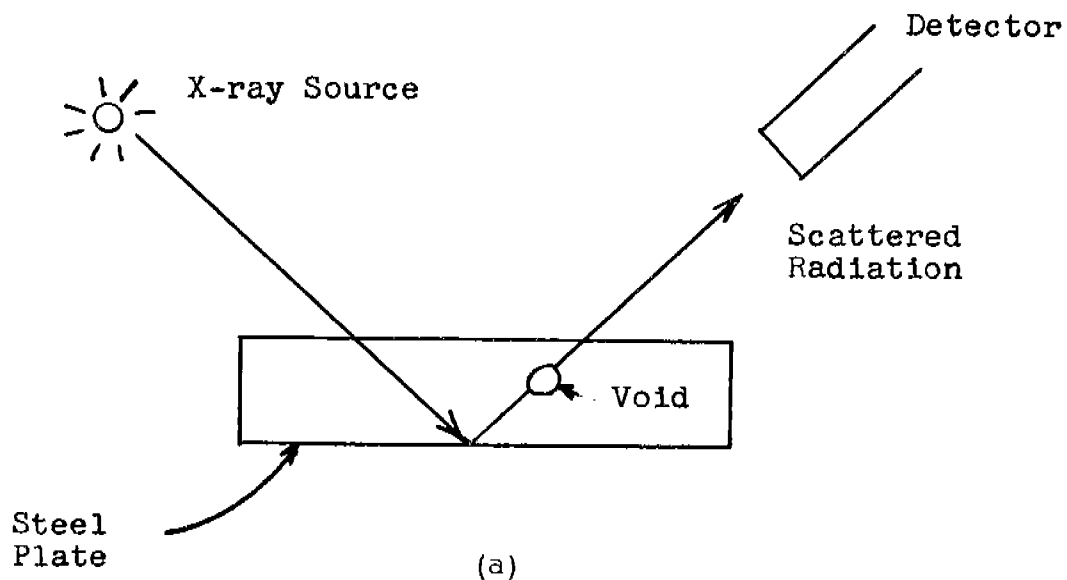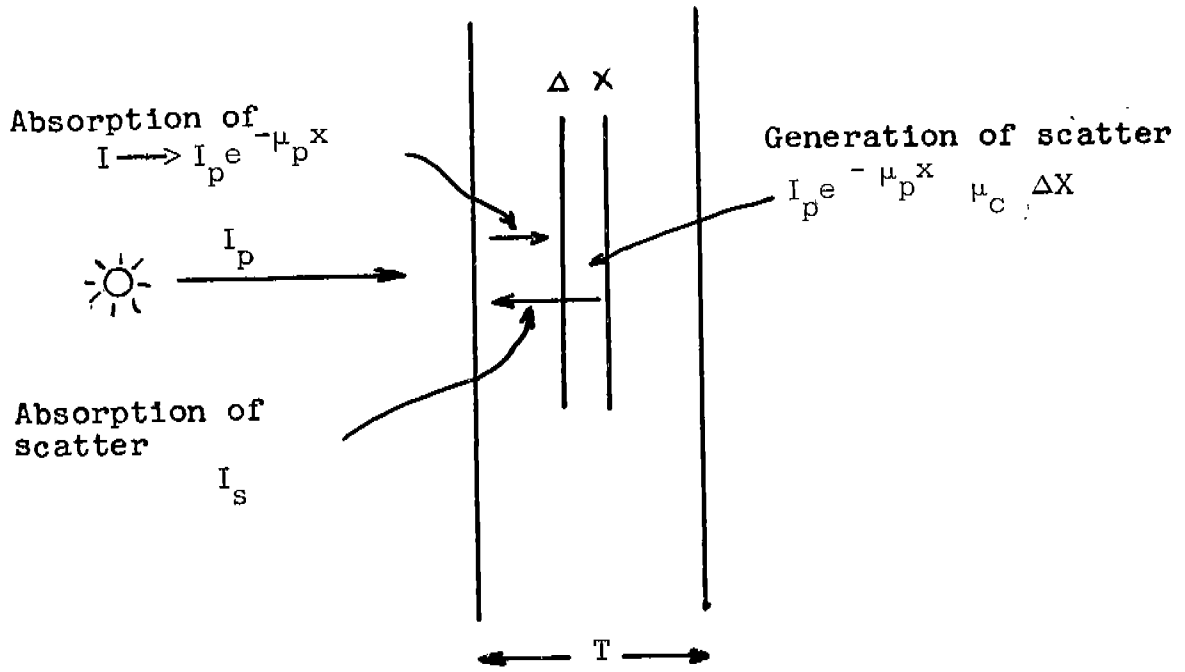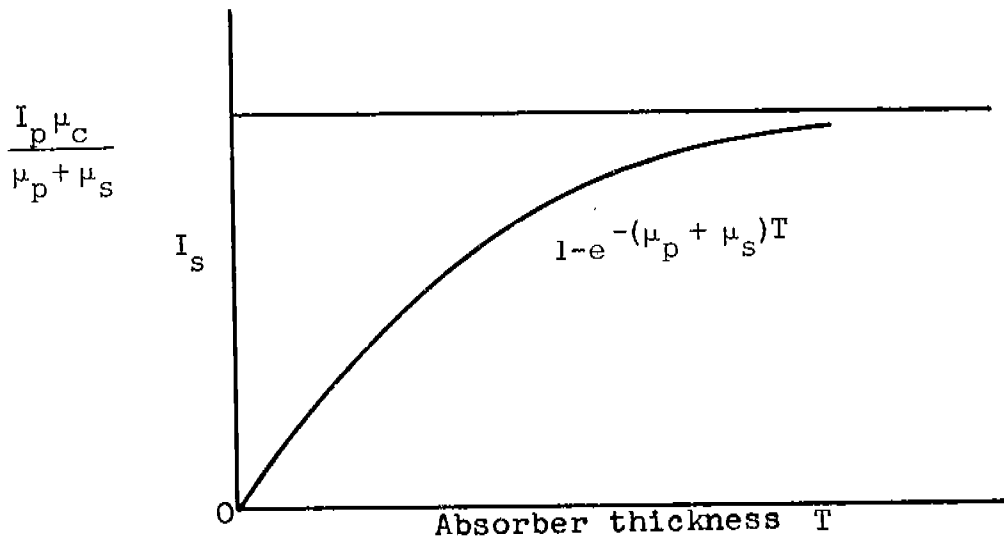$$\Delta I_s = I_p e^{(\mu_p + \mu_s)x} \mu_c \Delta x$$

FIG. 1. X-RAY INSPECTION ARRANGEMENTS THAT MEASURE THE ATTENUATION OF BACK SCATTER RADIATION BY MEANS OF A SCINTILLATION COUNTER (a) OR PINHOLE CAMERA (b).

Absorption of $I \longrightarrow I_p e^{-\mu_p x}$

I_p

ΔX

Generation of scatter

$I_p e^{-\mu_p x} \mu_c \Delta X$

Absorption of scatter I_s

T

(a)

$\dfrac{I_p \mu_c}{\mu_p + \mu_s}$

I_s

$1 - e^{-(\mu_p + \mu_s)T}$

0

Absorber thickness T

(b)

FIG. 2. ILLUSTRATION (a) SHOWING RELATIONSHIP OF TERMS IN DEVELOP-
MENT OF EQ. 1 FOR SCATTERED INTENSITY, AND SKETCH (b) INDICATING THE
SCATTERED INTENSITY AS A FUNCTION OF THE THICKNESS OF THE PLATE.

where

I_p = primary intensity

I_s = scattered intensity

μ_p = linear absorption coefficient of the primary beam

μ_s = linear absorption coefficient of the scattered beam

μ_c = scattering coefficient

T = absorber thickness

and therefore,

$$I_s = I_p \int_0^T e^{-(\mu_p + \mu_s)x} \, \mu_c \, dx$$

(1)

$$I_s = \frac{I_p \, \mu_c}{\mu_p + \mu_s} \left[1 - e^{-(\mu_p + \mu_s)T} \right]$$

A sketch of this equation is shown in Fig. 2(b). This shows the scattered intensity as a function of thickness of absorber T. As the thickness increases there is little additional scatter contributed from the last increments of absorber. The scatter for large thicknesses approaches a value of $\frac{I_p \, \mu_c}{\mu_p + \mu_s}$. The general shape of this curve indicates that there is a practical thickness limit.

Detectability of Voids

In radiography where the film and sources of radiation are on opposite sides of the object, sensitivity is used as a general measure of void detectability. Sensitivity is expressed as $\frac{\Delta x}{x}$ with a fixed relationship between Δx and hole diameter. Since conventional sensitivity measurements cannot conveniently be applied to the scattered-radiation method, it is simpler to consider the void-size detectability as a function of its depth with the object.

Contrast is proportional to the per cent change in intensity:

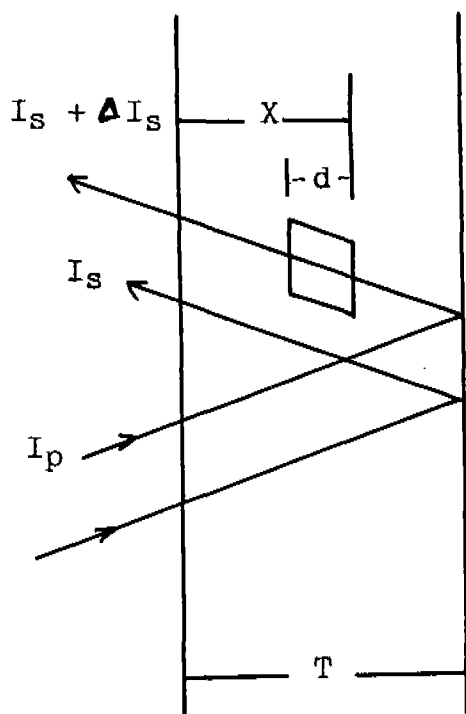$$\text{Contrast} \simeq \frac{\Delta I}{I} \times 100$$

FIG. 3. DIAGRAM TO AID IN
THE DEVELOPMENT OF EQ. 2
WHICH DETERMINES THE CHANGE
IN SCATTERED RADIATION PRO-
DUCED BY A VOID.

In imaging with scattered radiation, the contrast produced by a void is a function of depth. A void on the front surface would have the maximum contrast, whereas a void in the middle of an object would have a lower contrast because the material in front of the void produces scatter.

Assume a void $\underline{d}$ is located in a volume at a distance $\underline{X}$ from the front surface (Fig. 3). The change in scattered radiation produced by the void is equal to the difference between the scatter from a volume with a void and that from a volume without a void. An expression for ΔI can be derived as follows:

Scatter generated behind the void as detected at the front surface is

$$I_{s_2} = I_p \mu_c \; e^{-\mu_p X} \; e^{-\mu_s (X-d)} \int_0^{T-X} e^{-(\mu_p + \mu_s)(x)} dx$$

(2)

$$I_{s_2} = \frac{I_p \mu_c}{\mu_p + \mu_s} \left[e^{-(\mu_p + \mu_s)X} - e^{-(\mu_p + \mu_s)T} \right] e^{\mu_s d}$$

The scatter produced in front of a void as detected on the front surface is

$$I_{s_1} = I_p\mu_c \left[1 - e^{-(\mu_p + \mu_s)(X-d)}\right] \Big/ \mu_p + \mu_s$$

and the scatter produced with no void is

$$I_s = I_p\mu_c \left[1 - e^{-(\mu_p + \mu_s)T}\right] \Big/ \mu_p + \mu_s$$

therefore

$$\Delta I_s = I_s - I_{s_1} - I_{s_2}$$

$$\Delta I_s = I_p\mu_c \left\{ e^{-(\mu_p + \mu_s)X}\left(e^{(\mu_p + \mu_s)d} - e^{\mu_s d}\right) \right.$$

$$\left. + e^{-(\mu_p + \mu_s)T}\left(e^{\mu_s d} - 1\right)\right\} \Big/ \mu_p + \mu_s \tag{3}$$

$$\Delta I_s/I_s = \left\{ e^{-(\mu_p + \mu_s)X}\left(e^{(\mu_p + \mu_s)d} - e^{\mu_s d}\right) \right.$$

$$\left. + e^{-(\mu_p + \mu_s)T}\left(e^{\mu_s d} - 1\right)\right\} \Big/ \left\{1 - e^{-(\mu_p + \mu_s)T}\right\} \tag{4}$$

The relationship between density and X-ray intensity is as follows:

D = m log I T

D = film density

m = film gradient

I = X-ray intensity

T = exposure time

$$\Delta D = \frac{m}{2.3} \quad \frac{\Delta I}{I}$$

The generally accepted minimum perceptible density difference is $\Delta D = 0.010$. For the film-screen combination used in this type of experiment, $m \approx 1.5$, and

therefore $\Delta I/I = (.010)(2.3)/1.5 = 0.015$. Putting this value into Eq. 4, X, the maximum depth at which a void $\underline{d}$-thick can be detected, is seen to be

$$X = \frac{1}{\mu_p + \mu_s} \ln \frac{e^{\mu_s d}\ (e^{\mu_p d} - 1)}{.015\left(1 - e^{-(\mu_p + \mu_s)T}\right) - (e^{\mu_s d} - 1)\ e^{-(\mu_p + \mu_s)T}} \qquad (6)$$

The above equation shows that the minimum detectable thickness is a function of μ_p, μ_s, and $\underline{m}$. A plot of this equation for typical values of μ_p, μ_s and m is useful to visualize the relation between $\underline{d}$ and X. An assumption of a steel-plate thickness T of one inch is satisfactory, since ship welds range in thickness from 1/2 to 1.5 in. Experimental results presented later in this report indicate the following values for μ_p and μ_s:

Primary Source (kv)	μ_p (in.$^{-1}$)	μ_s (in.$^{-1}$)
250	2.8	17
400	2.2	5.5
2000	0.92	2.5

The above values were inserted into Eq. 7 and a set of curves was plotted as shown in Fig. 4. From this graph it can be seen that a 0.1-in. void is detectable at a depth of 0.24 in. at 250 kv, 0.43 in. at 400 kv, and 0.98 in. at 2000 kv. These curves are very optimistic since they do not consider the angles of the radiation and the radiation leakage into the camera or detector.

EXPERIMENTAL DATA ON SCATTERED RADIATION

General

The proper selection of source-object and source-camera angles is dependent upon the intensity and energy of the scattered radiation emitted from the steel plate. Intensity distribution and energy of the secondary radiation vary as a function of plate material, primary energy, and angle of the plate with respect
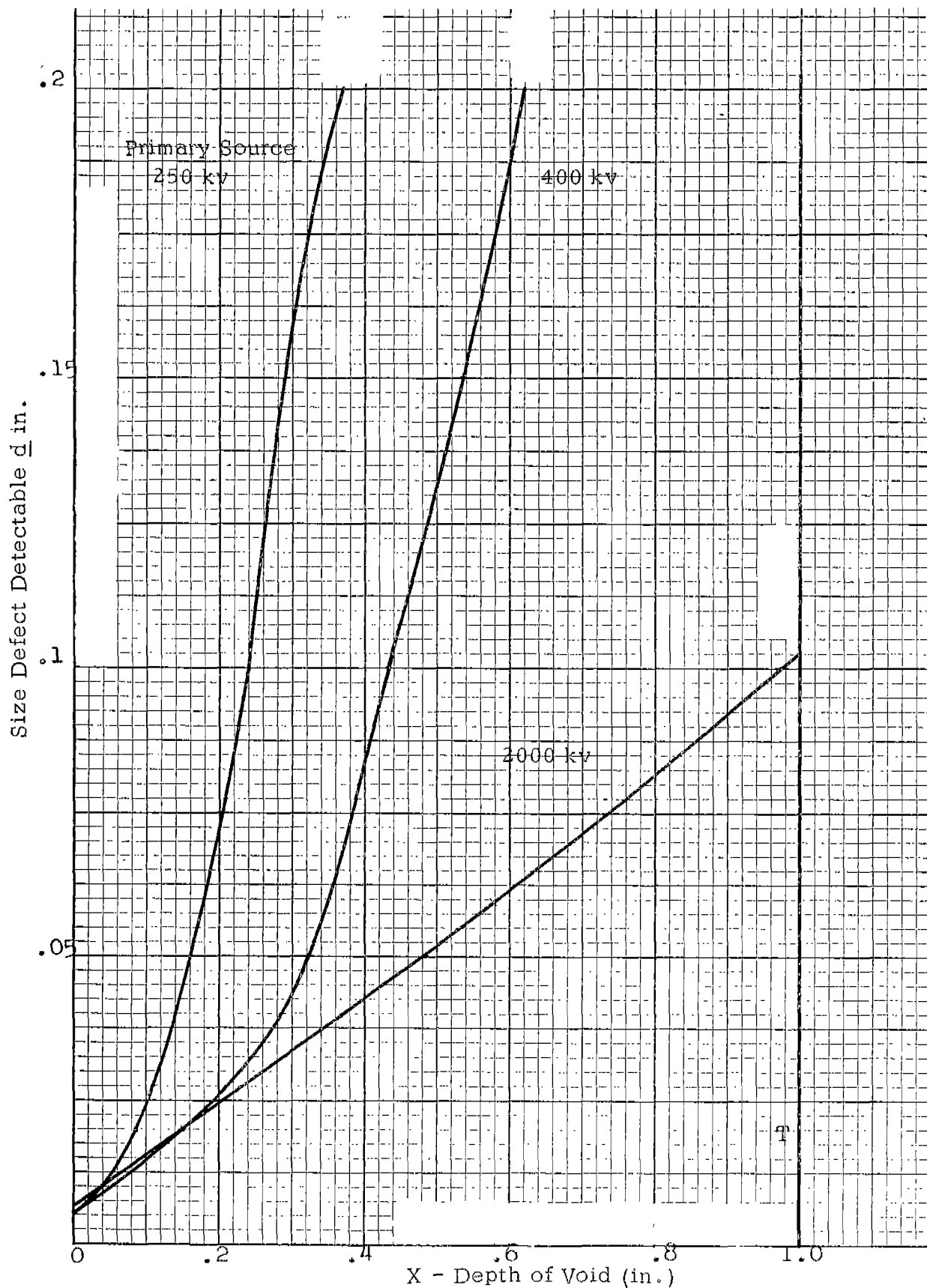
FIG. 4. DETECTABILITY OF VOID AS A FUNCTION OF PLATE DEPTH.
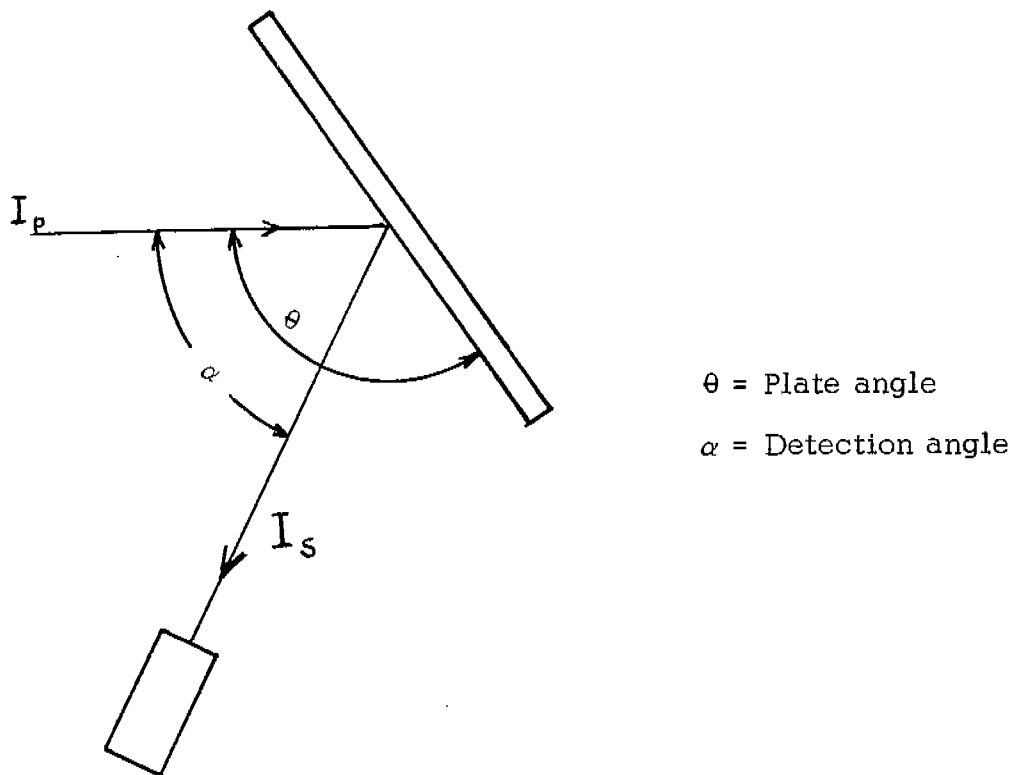
θ = Plate angle

α = Detection angle

FIG. 5. ARRANGEMENT FOR MEASURING PLATE AND DETECTOR ANGLES.

to the primary beam. Experimental data were taken with a 1-in. steel plate excited by 250 kv, 400 kv, 2000 kv, Cobalt 60, and Cesium 137 sources. A photomultiplier tube with a phosphor was used to measure the relative intensity of the scattered radiation; at low energies a ZnS screen was used, at high energies a sodium-iodide crystal.

Intensity Distribution

The intensity distribution was measured as shown in Fig. 5. The plate angle was varied from 45° to 150° relative to the primary source. At each plate angle the detector was moved through an arc from 15° to the angle at which the plate was set. The detector was shielded from the primary beam so that current in the phototube resulting from this source was at a minimum. Before a plot of the results was made, the background current was subtracted from the total reading. Relative intensities are shown in Figs. 6, 7, 8, 9, and 10 for 250 kv, 400 kv, 2000 kv, Cesium 137, and Cobalt 60, respectively.
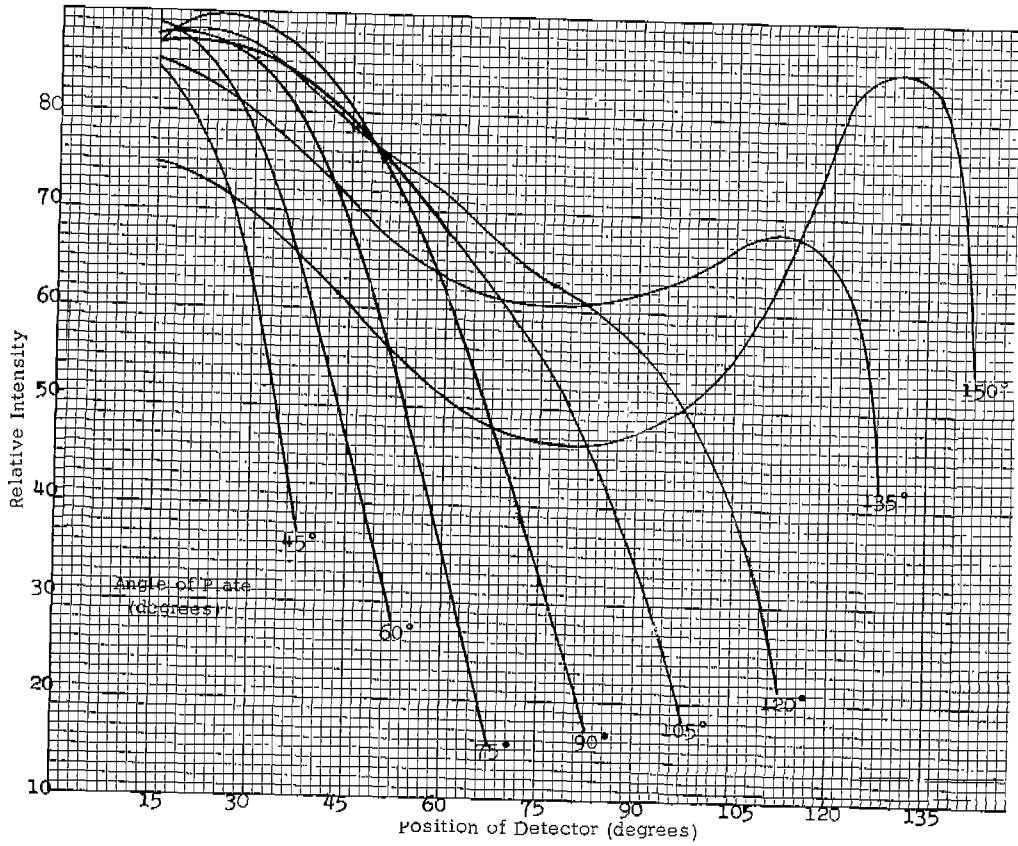
FIG. 6. INTENSITY DISTRIBUTION OF SCATTERED RADIATION USING A
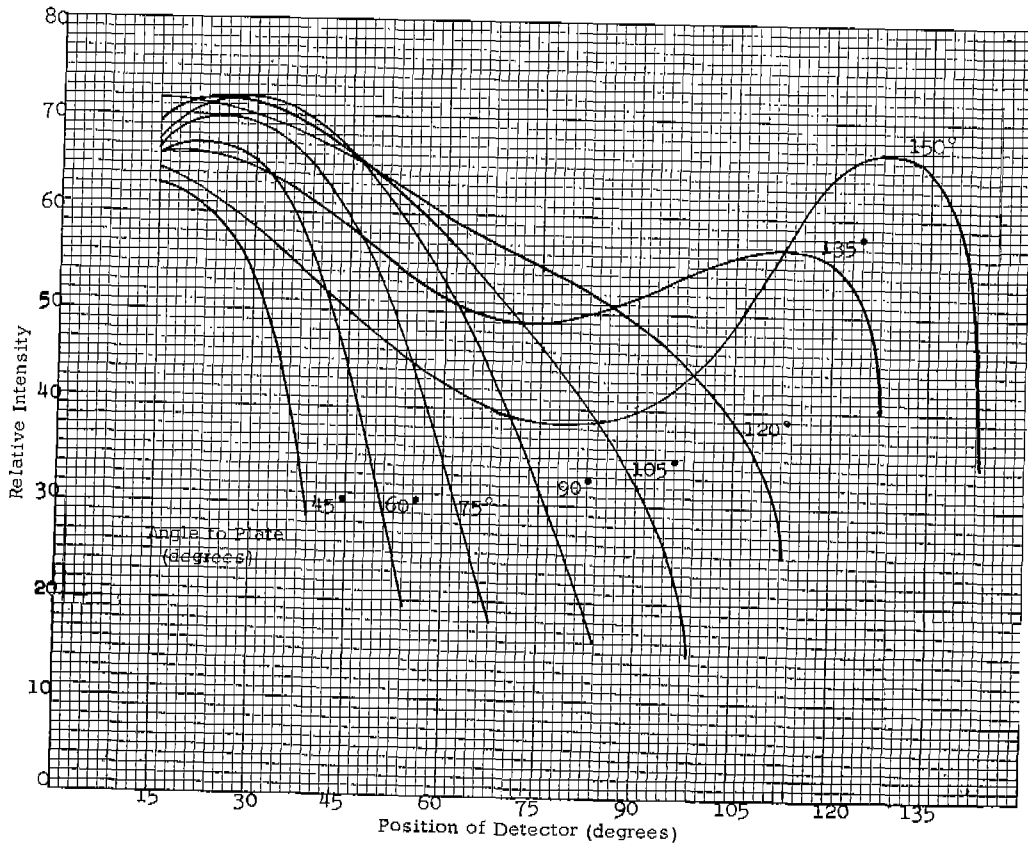PRIMARY SOURCE OF 250 KV.

FIG. 7. INTENSITY DISTRIBUTION OF SCATTERED RADIATION USING A
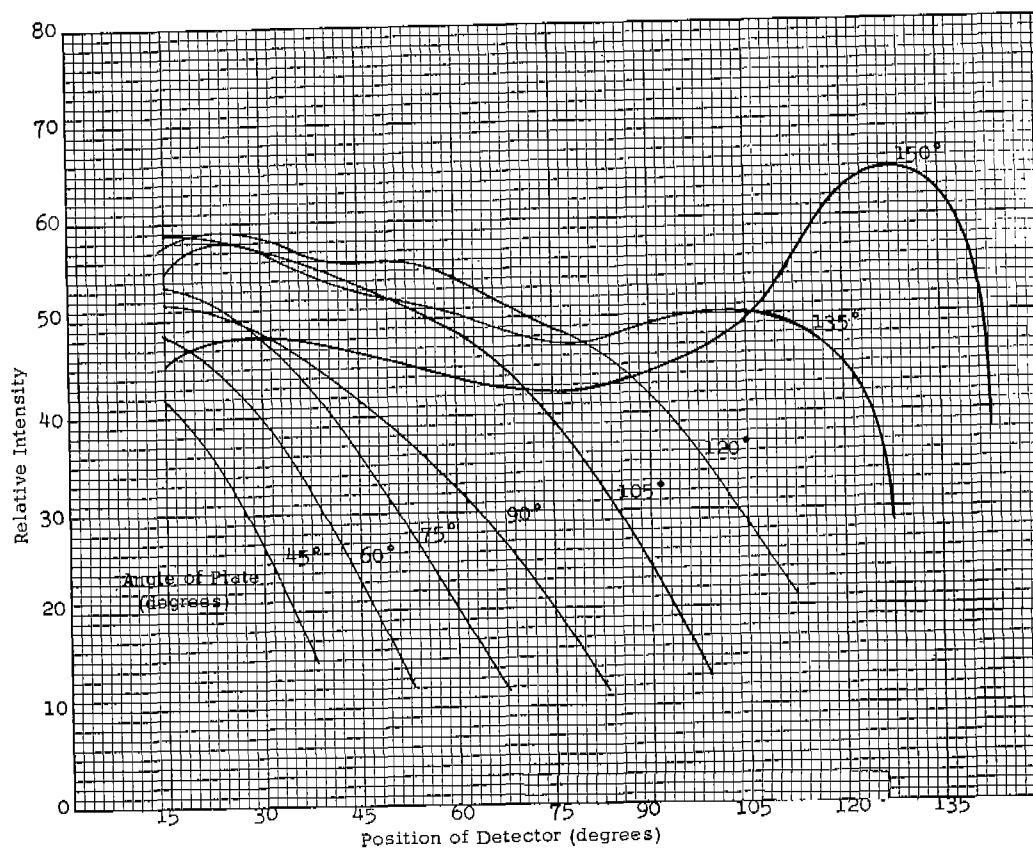PRIMARY SOURCE OF 400 KV.

FIG. 8. INTENSITY DISTRIBUTION OF SCATTERED RADIATION USING A PRIMARY SOURCE OF 2000 KV.
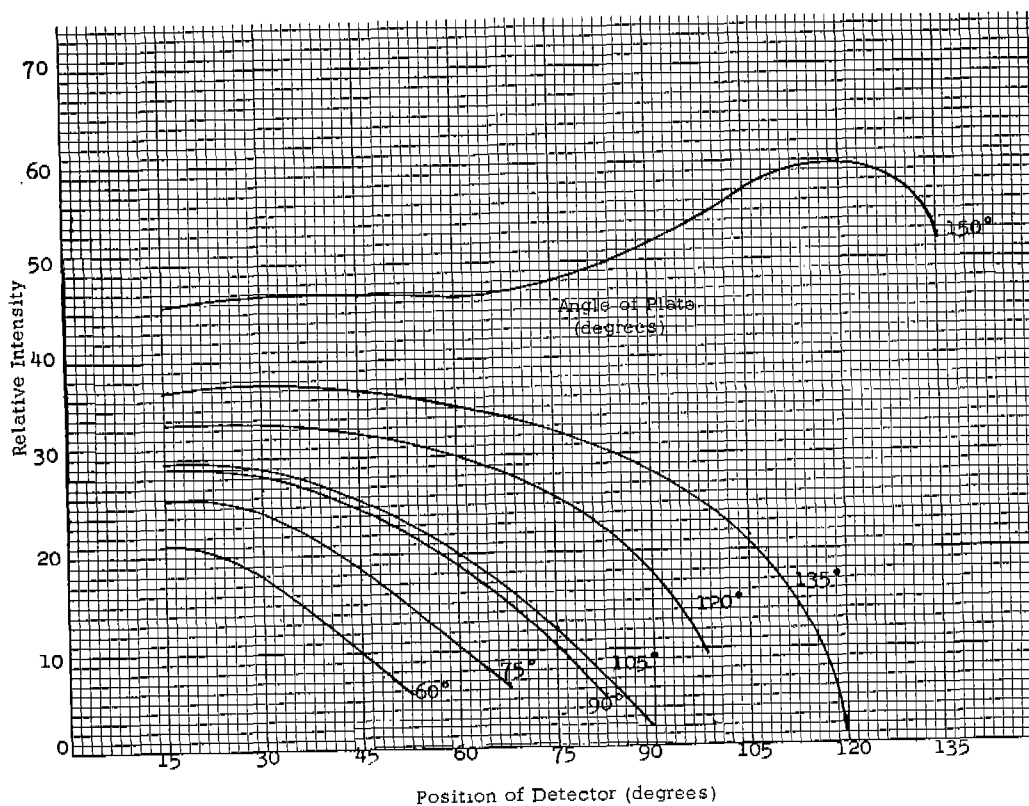

FIG. 9. INTENSITY DISTRIBUTION OF SCATTERED RADIATION USING A PRIMARY SOURCE OF CESIUM 137.
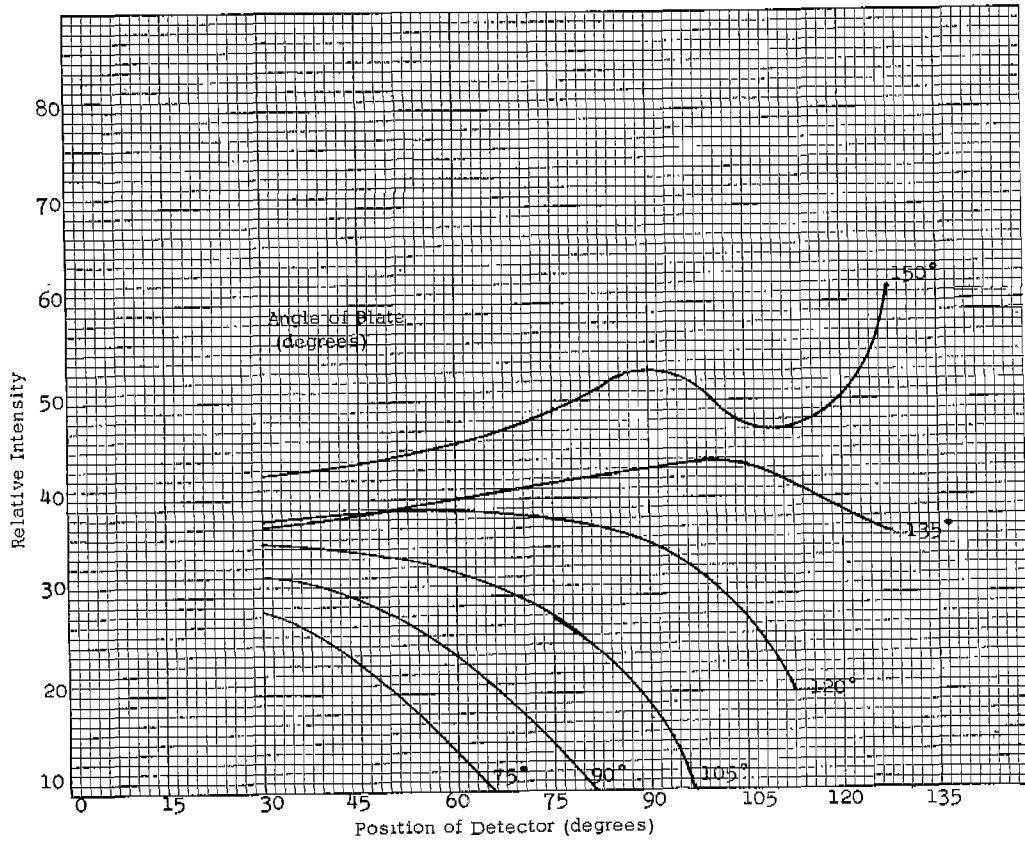
FIG. 10. INTENSITY DISTRIBUTION OF SCATTERED RADIATION USING A PRIMARY SOURCE OF COBALT 60.

The plate and detector angles measured at maximum intensities for the various sources are given in Table I.

TABLE I

PLATE AND DETECTOR ANGLES FOR MAXIMUM SCATTERED INTENSITY

Energy	Plate Angle (°)	Detector Angle (°)
250 kv	90	30
400 kv	90	30
Cs 137	150	115
2000 kv	150	125
Co 60	150	125

Although the angles listed in Table I give the maximum intensity, another factor had to be considered before angles could be selected for pinhole camera imaging. This was the uniformity of field received through 10° to 15°. Angles
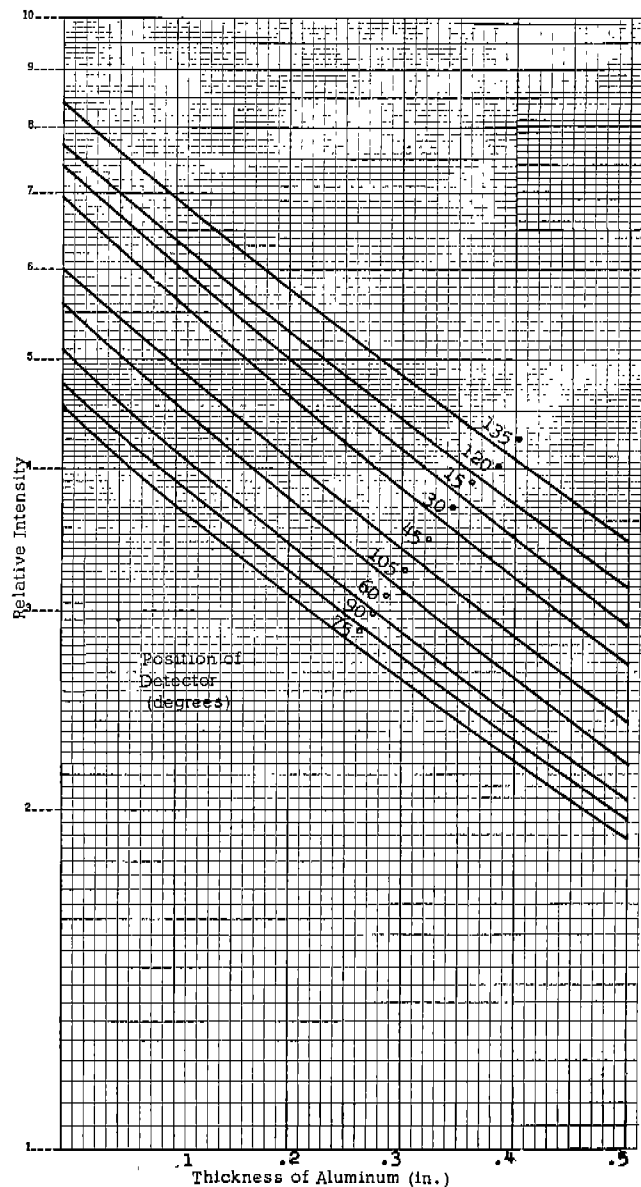
—

FIG. 11. ABSORPTION CURVE FOR
SCATTERED RADIATION USING A PRI-
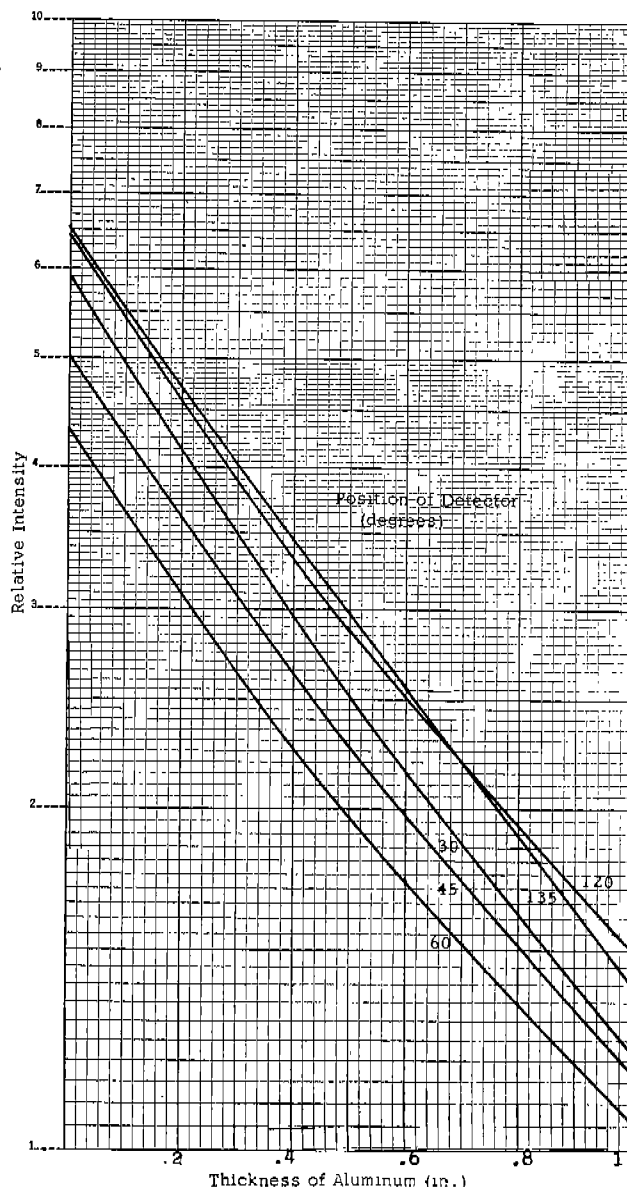MARY SOURCE OF 250 KV AND A PLATE
ANGLE OF 150°.

FIG. 12. ABSORPTION CURVE FOR
SCATTERED RADIATION USING A PRI-
MARY SOURCE OF 400 KV AND A PLATE
ANGLE OF 150°.

of 90° for detector and 135° for plate seemed to be best.

Energy Measurement

In addition to the intensity distribution, data were obtained on the
quality of the scattered radiation. The same physical setup was used as in
making intensity measurements, but various absorber thicknesses were added
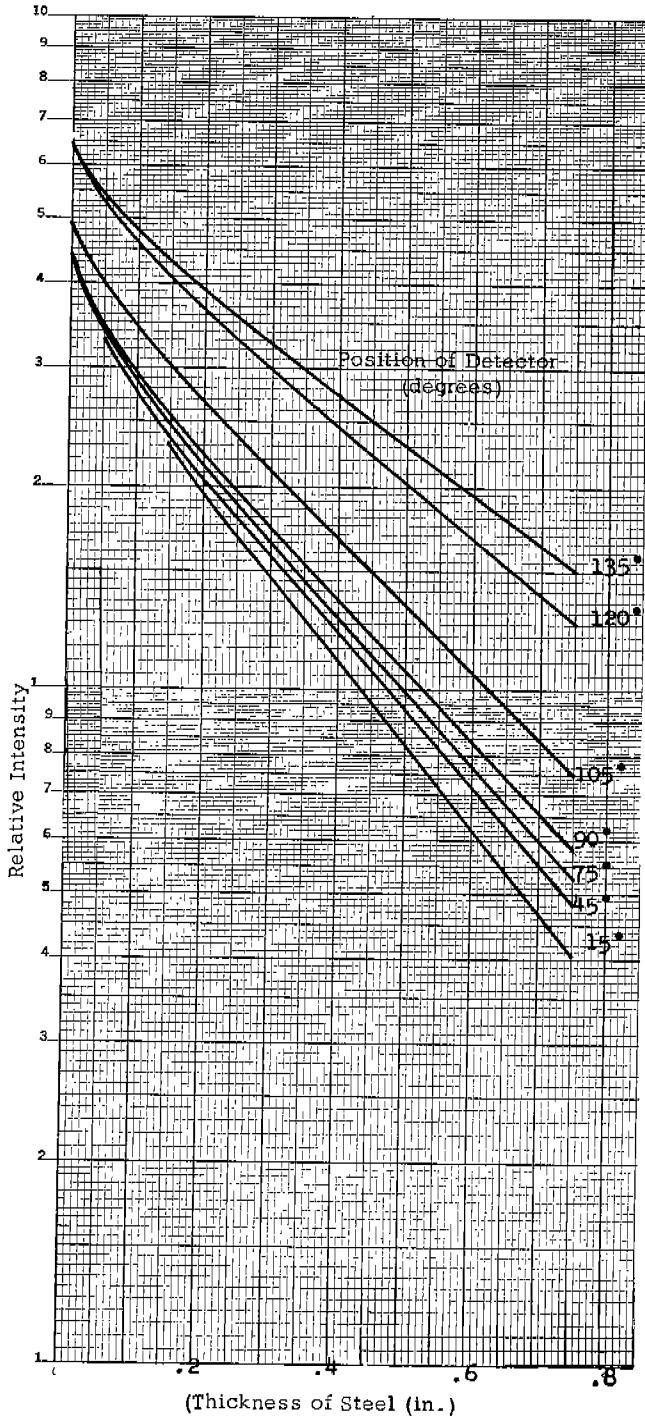in front of the detector. From this information the absorption curves for scat-

FIG. 13. ABSORPTION CURVE FOR
SCATTERED RADIATION USING A
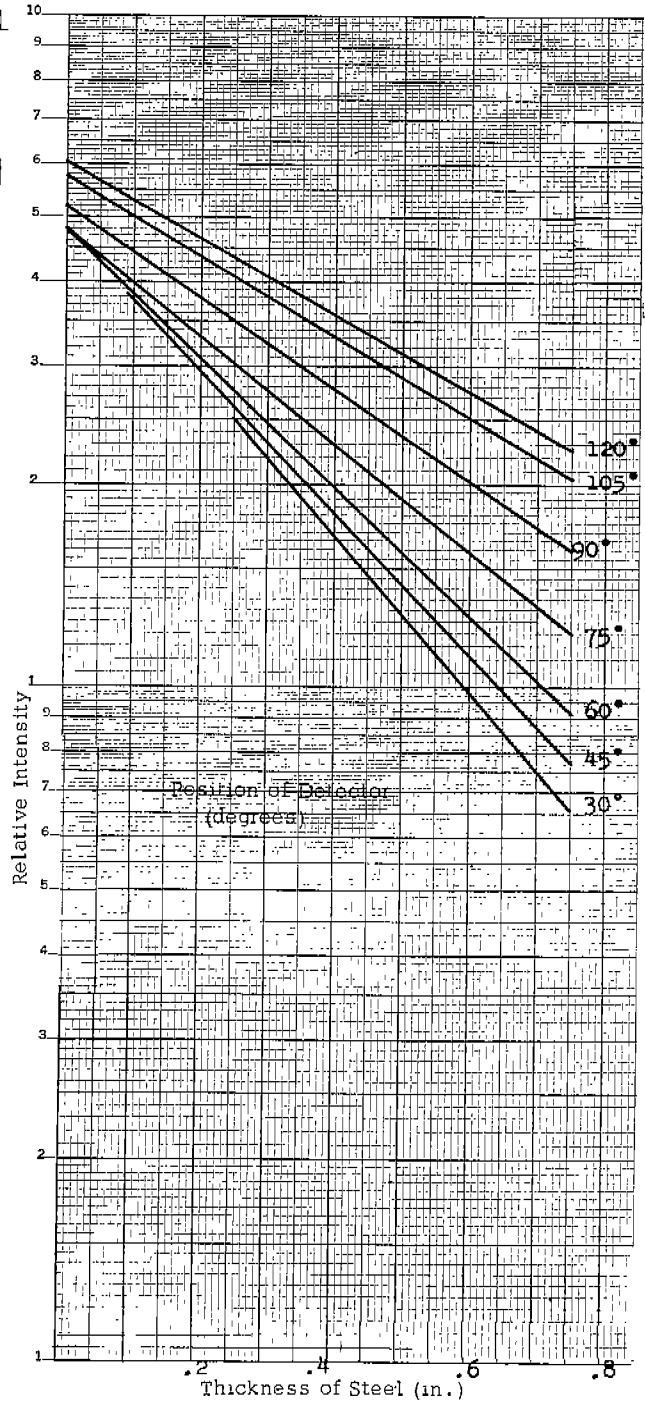PRIMARY SOURCE OF 2000 KV AND
A PLATE ANGLE OF 150°.

FIG. 14. ABSORPTION CURVE FOR
SCATTERED RADIATION USING A
PRIMARY SOURCE OF CESIUM 137
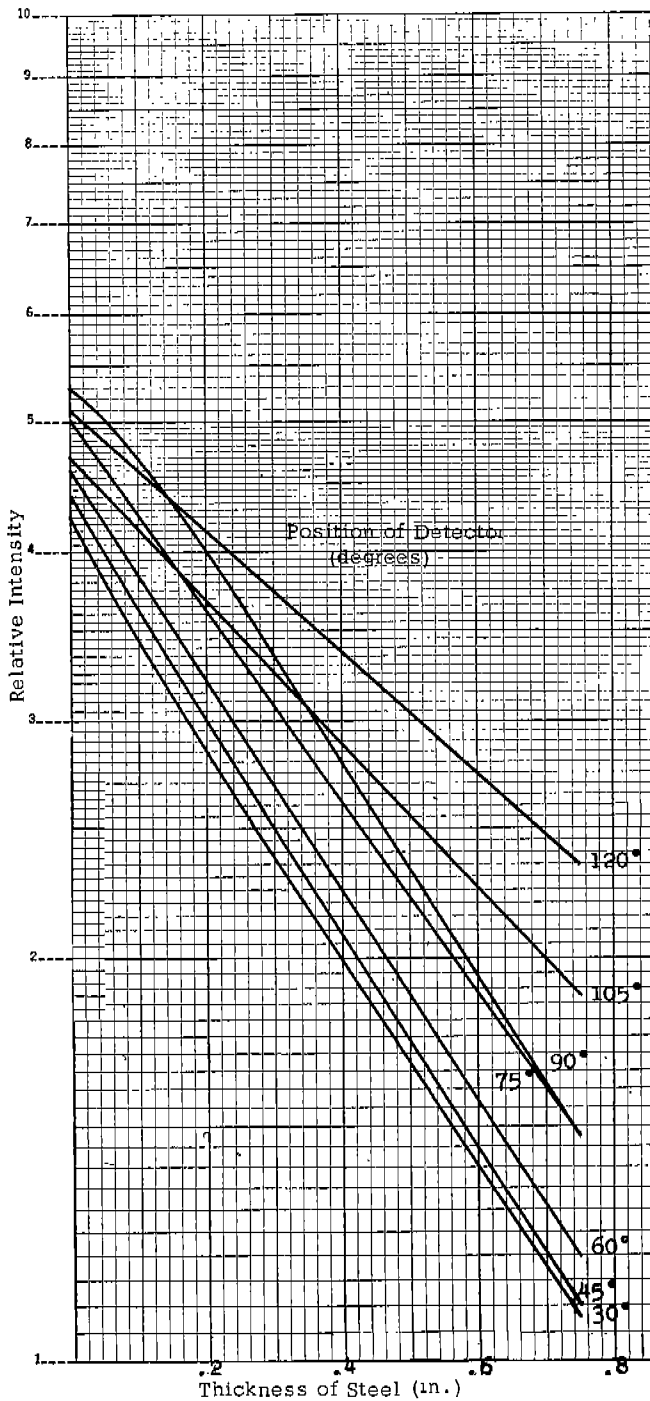AND A PLATE ANGLE OF 150°.

FIG. 15. ABSORPTION CURVE FOR
SCATTERED RADIATION USING A
PRIMARY SOURCE OF COBALT 60
AND A PLATE ANGLE OF 150°.

tered radiation were plotted as shown in Figs. 11-15.

Since the energy of the scattered radiation was in the order of 50 to 100 kv for 250 or 400 kv excitation, aluminum was used as the absorption material. For higher voltages, steel was used as the absorber. Table II shows the half-value thicknesses and energy obtained from the above absorption curves. From the half-value thicknesses the linear absorption coefficients μ_p and μ_s were determined. The last column of this table gives the sum of μ_p and μ_s, which is used in the detectability curve.

Scatter as a Function of Plate Thickness

Theoretical information on the generation of scatter as a function of plate thickness was presented in a previous section. Experiments were conducted to verify the shape of the curve and to see if a fit of the data could be made to the equation. The same apparatus as described in the section on intensity measurements was used for this experiment. At 250 kv the detector and plate angles were set at 90° and 135°, respectively; at 2000 kv the detector angle was 45° and the plate angle 105°. The steel-plate thickness was varied from 0 to 2 in. while the intensity was recorded.

TABLE II

DETECTOR ANGLE 90°--PLATE ANGLE 150°				
Primary Source (kv)	HVL (in.)	Linear Absorption Coefficient (in.$^{-1}$)		
		μ_p	μ_s	$\mu_p + \mu_s$
250	.375 Al	2.8	17.0*	19.8
400	.540 Al	2.2	5.5*	7.7
2000	.275 Fe	0.92	2.5	3.42

*Estimated from ratio of HVL of Fe and Al[3]

A plot of the results obtained at 250 kv and 2000 kv is shown in Figs. 16 and 17. Equation 1 states that

$$I_s = I_p \mu_c \left[1 - e^{-(\mu_p + \mu_s)T} \right] / \mu_p + \mu_s$$

It was found that the following values of $(\mu_p + \mu_s)$, when inserted into the above equation, fit the experimental data.

Source	$\mu_p + \mu_s$
250 kv	20
2000 kv	2.9

These results check with the information presented in Table II and indicate that $\mu_p + \mu_s$ are of the right order of magnitude.

PINHOLE CAMERA

General

The pinhole camera, similar to the type used with light, can be applied to resolve an image from a source of X- or gamma-radiation.[4-6] Penetrating radiation presents a number of problems, since the radiation cannot be completely stopped
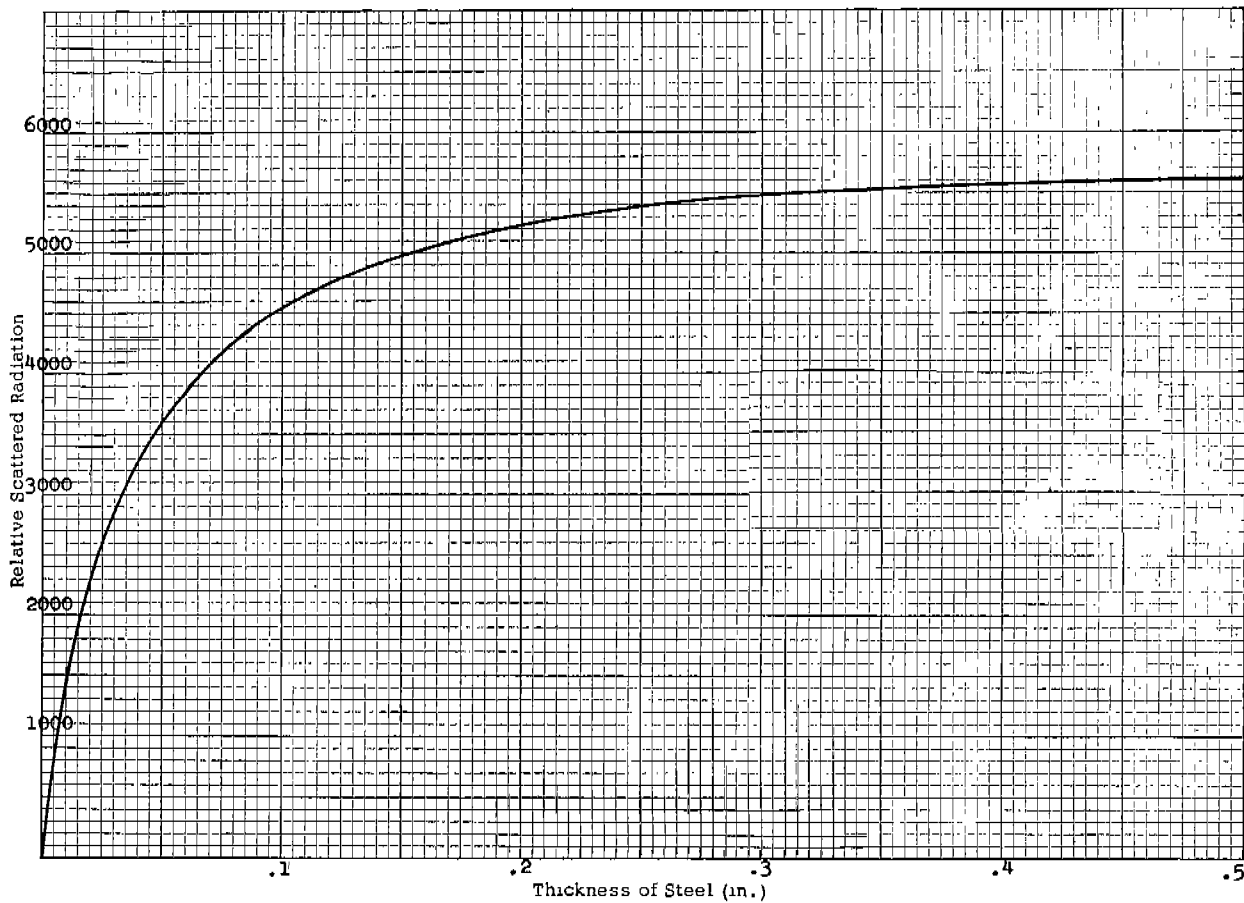
FIG. 16. SCATTERED RADIATION AS A FUNCTION OF PLATE THICKNESS, USING A PRIMARY SOURCE OF 250 KV, A DETECTOR ANGLE OF 90° AND A PLATE ANGLE OF 135°.
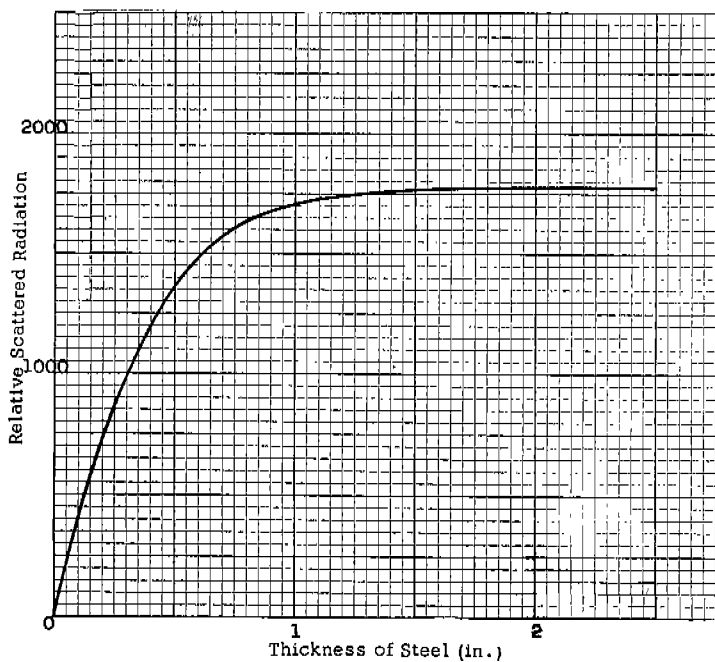

FIG. 17. SCATTERED RADIA-TION AS A FUNCTION OF PLATE THICKNESS USING A PRIMARY SOURCE OF 2000 KV, A DETEC-TOR ANGLE OF 45° AND A PLATE ANGLE OF 105°.
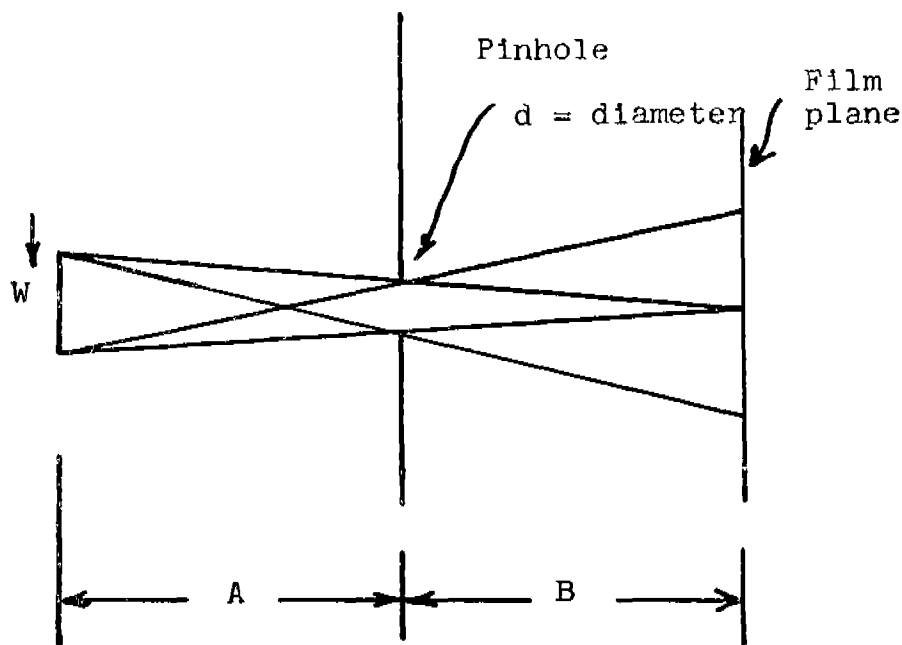
Pinhole

d = diameter

Film
plane

W

A

B

FIG. 18. GEOME-
TRIES INVOLVED TO
REMOVE THE UMBRAL
(SHADOW) IMAGE.

by the walls of the camera. This radiation leakage results in reduced image contrast and poor resolution. This problem and others can be partially over-come by careful camera design.

Pinhole Design

The ideal pinhole transmits 100 per cent of the gamma radiation through the hole and none through the surrounding material. With penetrating radiation this ideal situation cannot be achieved. In practice, a wall thickness that re-duces the radiation to 1 per cent of the original value is satisfactory; this rep-resents about 7 half-value thicknesses of material. Table III gives the half-value thicknesses for lead and also the thickness required for 7 half-value thicknesses at various X-ray voltages. The wall thickness for the camera at any given X-ray energy can be selected from Table III. Another factor to consider is resolution: this is affected by diameter of the pinhole and dis-tance of the pinhole from object and film. Figure 18 shows the geometries in-volved where the umbral image vanishes. If it is assumed that this is the limit of resolution, then

$$W = d \frac{A + B}{B}$$

where

> W = width of the smallest size defect resolvable
>
> d = effective diameter of pinhole
>
> A = distance from the pinhole to object
>
> B = distance from pinhole to film

TABLE III

Voltage (kv)	Half-Value Thickness (in.) Pb	Thickness for 7 half-value thicknesses (in.) Pb
250	0.022	0.144
400	0.040	0.28
1000	0.20	1.40
2000	0.5	3.5

In optics, the "speed" of a lens is rated in terms of an "f" number, which is the ratio of focal length to diameter of the lens. The same relation can be established for a pinhole lens.

$$f = B/d$$

as a result, the previous relationship becomes

$$W = \frac{A + B}{f}$$

and, since A + B is equal to the distance from object to film (D),

$$W = D/f$$

This equation shows that the width of defect that can be resolved must be equal to or greater than D/f. As the camera is moved away from the object, the smallest defect that can be resolved must be larger.
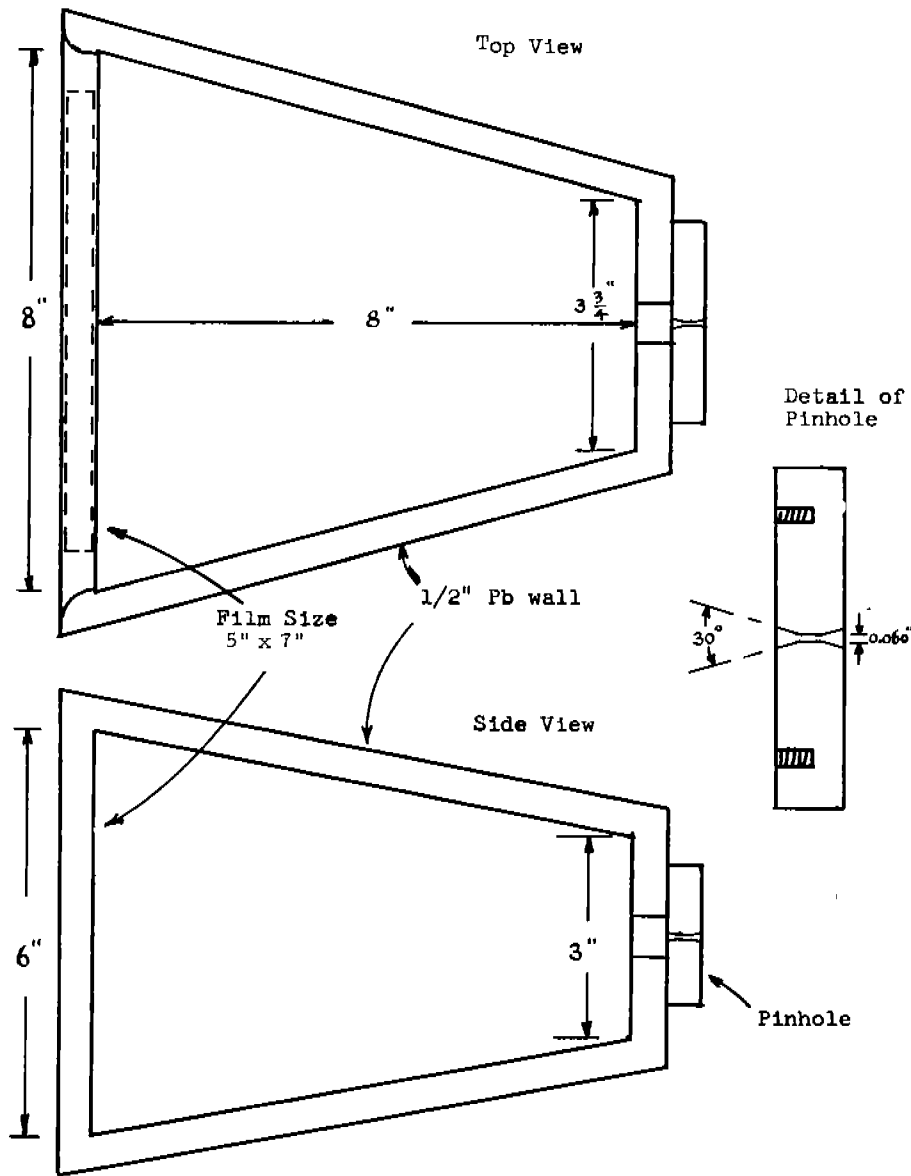
Top View

8"

8"

3 3/4"

Detail of Pinhole

Film Size 5" x 7"

1/2" Pb wall

30°

0.060"

Side View

6"

3"

Pinhole

FIG. 19. SKETCH OF PINHOLE CAMERA.

Experimental Camera

Since the experimental work covered the energy range from 250 to 2000 kv, the pinhole camera had to image satisfactorily through this energy range. (Figure 19 is a sketch of the camera.) The top of the camera was made so that the film was easily accessible. It holds standard 5 x 7-in. X-ray film. The lead walls are 1/2 in. thick; lead bricks are piled around the camera to provide the additional shielding required for the higher energy ranges. The pinhole was made of a tungsten-copper sintered material (commercial HEVIMET), which has a density of 19 and better machining properties than lead. From the camera

FIG. 20. X-RAY IMAGE OF A WELDED PLATE SPECIMEN THAT SHOWS
A WELD WITH TWO PENETRAMETERS ALONGSIDE THE BEAD.

dimensions and pinhole size, the f number of the camera was computed to be 130. Therefore the minimum size defect that could be resolved at a distance of 24 in. is

$$W = D/f \text{ or } 24/130 \simeq 0.2$$

Images with Scattered Radiation

Experiments were conducted with the pinhole camera to establish the limitations of this system for the inspection of welds. The first attempts were directed toward obtaining an image of a simple object. Figure 20 shows an image of a weld with two penetrameters alongside the bead, the bead and penetrometers are well-defined, but there is little indication of sub-surface discontinuities within the weld. In order to obtain a better idea of the depth to which a discontinuity can be detected, a 1/16-in. (and then a 1/8-in.) steel plate were placed over the weld bead and penetrometers and images were made for each condition. These are shown in Figs. 21 and 22. The image of the weld bead and penetrometers is barely discernible when covered by the 1/8-in. steel plate. An exposure time of about 20 min was required, using 250 kv, Type-F film, calcium tungstate screens, and with the X-ray machine 13 in. and the camera 16 in. from the plate. The camera angle was 90° and the plate angle was 135°.

A similar study was conducted with a 1/4-in. steel plate containing several drilled holes of different diameters. Images were made of this plate covered by several thicknesses of steel. A 1-in. back plate was used at all times. It was found that the maximum depth at which a discontinuity was detectable is 0.2 in. at 2 million volts and about 0.125 in. at 250 kv.

The results for 250 kv agree within a factor of 2 with the information presented in Fig. 4. However, the 2000-kv data do not agree; this may be due to radiation leakage into the camera.

SUMMARY

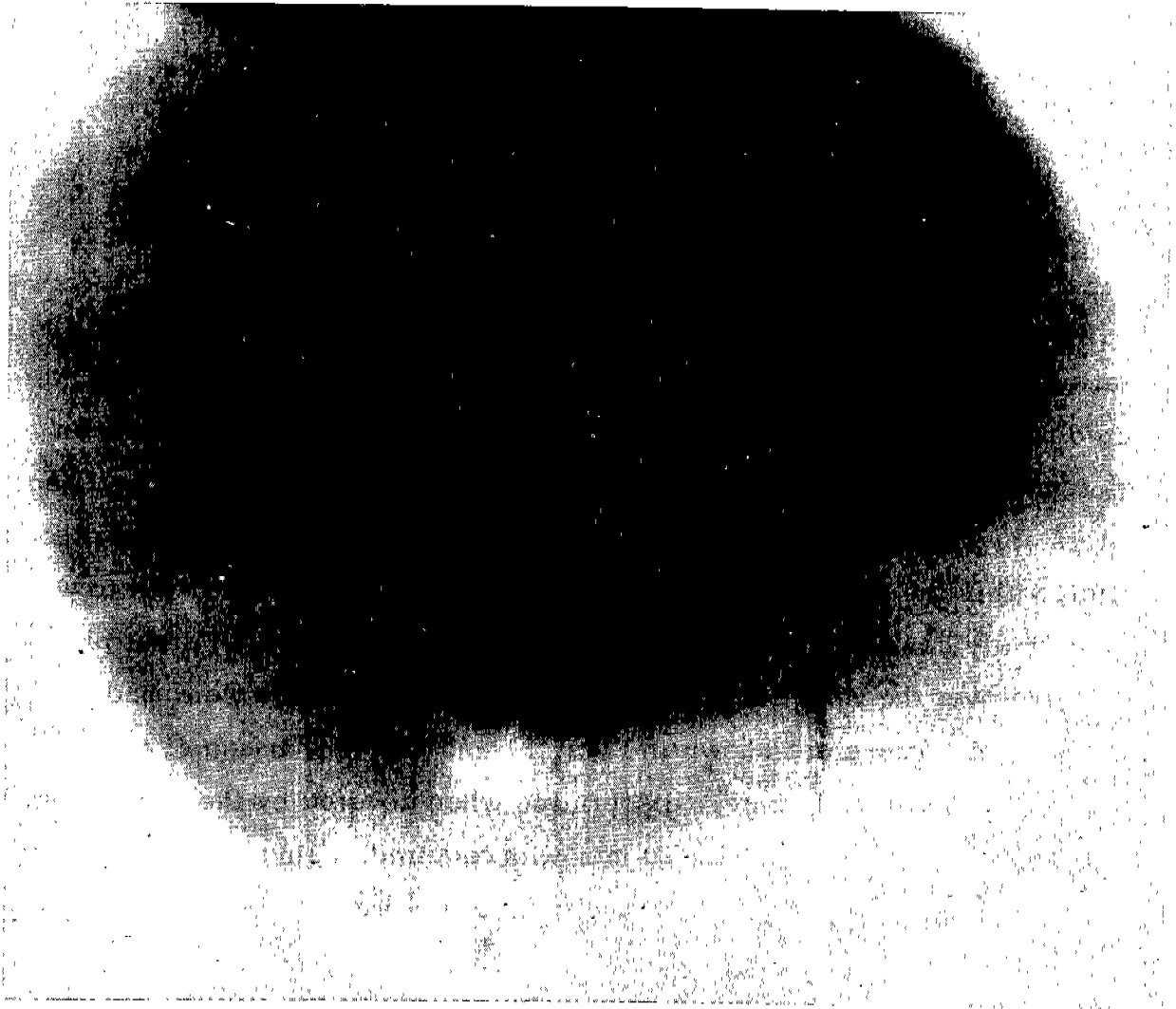As indicated by the theoretical and experimental work, there is a serious

FIG. 21. SAME PLATE AS SHOWN IN FIG. 20 EXCEPT A 1/16-IN. STEEL
PLATE WAS PLACED OVER THE WELD BEAD AND PENETROMETERS.

limitation on the depth at which discontinuities in steel can be detected. The
maximum depth at which a void was detectable was 0.20 in.

Another important consideration is exposure time. At 250 kv, 20 min
are required when the camera-object distance is 16 in. and there is no magni-
fication. At this energy it requires about 6000 roentgens incident on the sur-
face of the plate to obtain a satisfactory exposure.

In view of the limited depth of inspection and long exposure times, this
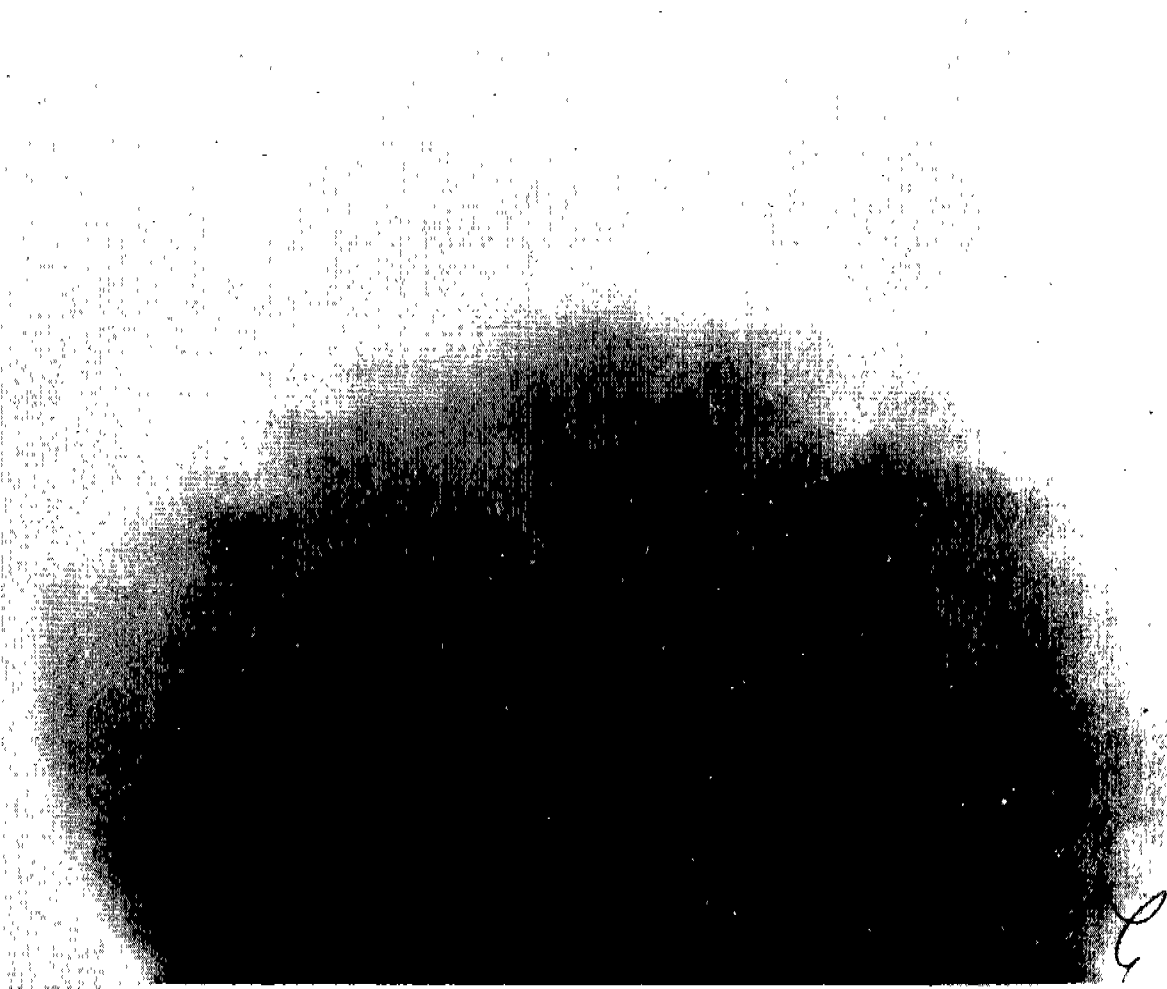approach is not considered very promising as a critical inspection tool.

FIG. 22. SAME PLATE AS SHOWN IN FIG. 20 EXCEPT A 1/8-IN. STEEL
PLATE WAS PLACED OVER THE WELD BEAD AND PENETROMETERS.

REFERENCES

1. Bujes, J. I., _Development of Filmless Technique for Recording Defects in Ship Welds_ (Ship Structure Committee Report Serial No. SSC-104), Washington: National Academy of Sciences-National Research Council, February 25, 1957. (Reprinted - July 11, 1958.)

2. Gravitte, Dwight L., _X-ray Backscattering Photography_ (ERDL Technical Report 1570 Confidential), Fort Belvoir, Va.: Engineering Research and Development Laboratories, February 1959.

3. _Handbook of Industrial Radiology_ (NAVORD Report 3649), White Oak, Md.: Naval Ordnance Laboratory.

4. Mortimer, R. K., Anger, H. O. and Tobias, C. A., _The Gamma-Ray Pinhole Camera with Image Amplifier_ (UCRL Report 2524), Berkeley, Calif.: University of California Research Laboratories, March 1954.

5. Copeland, D. E., and Benjamin, E. W., "Pinhole Camera for Gamma-Ray Sources," _Nucleonics_, 5:2, pp. 44-49 (1949).

6. Anger, H. O., "Use of a Gamma-Ray Pinhole Camera for _in-vivo_ Studies," _Nature_, vol. 170. p. 200 (1952).

SHIP STRUCTURE SUBCOMMITTEE

Chairman:

    J. J. Stilwell, Capt., USN
    Head, Hull Design Division
    Bureau of Ships

Secretary:

    J. D. Crowley, LCDR. USCG
    Office of the Engineer-in-Chief
    U. S. Coast Guard

Members:

    T. J. Griffin
    Head, Metals Section
    Bureau of Ships

    John Vasta
    Chief, Hull Scientific Section
    Bureau of Ships

    Louis Olivari, LCDR, USN
    Assistant to Maintenance & Repair Officer
    Military Sea Transportation Service

    Hubert Kempel
    Head, Technical Branch
    Military Sea Transportation Service

    J. B. Robertson, Jr.
    Deputy Technical Assistant to Chief
    Merchant Marine Technical Division, USCG

    V. L. Russo
    Deputy Chief, Office of Ship Construction
    Maritime Administration

    W. G. Frederick
    Naval Architect (Structural)
    Maritime Administration

    D. B. Bannerman, Jr.
    Chief Surveyor - Hull
    American Bureau of Shipping

    G. W. Place
    Principal Surveyor, Metallurgy - Research
    American Bureau of Shipping